Improved AdS/QCD model with matter

Alexander Stoffers and Ismail Zahed

Phys. Rev. D **83**, 055016 — Published 24 March 2011

DOI: 10.1103/PhysRevD.83.055016

Improved AdS/QCD Model with Matter

Alexander Stoffers and Ismail Zahed

Department of Physics and Astronomy, Stony Brook University, Stony Brook NY 11794

Abstract

We study an improved AdS/QCD model at finite temperature and chemical potential. An Ansatz for the β-function for the boundary theory allows for the derivation of a charged dilatonic black hole in bulk. The solution is asymptotically RN-AdS in the UV and $AdS_2 \times \mathbb{R}^3$ in the IR. We discuss the thermodynamical aspects of the solution. The fermionic susceptibilities are shown to deviate from the free fermionic limits at asymptotic temperatures despite the asymptotically free nature of the gauge coupling at the boundary. The Polyakov line, the temporal and spatial string tensions dependence on both temperature and chemical potential are also discussed.

1 Introduction

Non-perturbative QCD at finite chemical potential is still elusive. First principle formulations such as the lattice suffer from the sign problem [1]. Most non-perturbative formulations based on semiclassics such as the instanton or dyon formulations require further insights on the role of the fermionic zero modes at finite chemical potential. Some insights on the role of the chemical potential at finite temperature can be gleaned from strong coupling lattice QCD [2] or models [3]. Most of these models for light 2-flavor QCD suggest a second order transition at small chemical potential and finite temperature, and a first order transition at higher chemical potential. Noteworthy is the occurence of a tricritical point which appears to be sensitive to the nature of the confining forces.

Non-perturbative QCD with a large number of colors at finite chemical potential is likely a crystal of confined baryons. The crystal binding energy can be parametrically small, causing it to melt under quantum fluctuations and/or temperature. The result is a strongly coupled baryonic liquid. The original Skyrme model supports this descriptive although it suffers from the inherent shortcomings of the higher order chiral terms at high density [4]. The chiral holographic approaches to QCD support the crystal structure in the large number of colors limit without the shortcomings of the Skyrme model [5]. The crystal is found to melt at relatively small temperatures by the Lindemann criterion, resulting into a holographic liquid of instantons at low density and dyons at higher densities. Therefore, it is reasonable to think that the cold and dense inhomogeneous phase gives way to a homogeneous phase under the effects of temperature.

The purpose of this work is to address issues in relation to the dense and hot homogeneous baryonic phase using the (bottom-up) holographic approach. Specifically, we will use a variant of the improved (bottom-up) holographic approach to finite temperature Yang-Mills in the large number of colors limit put forward by Gursoy et al. [6, 7, 8] with the addition of a fermion chemical potential to account for baryon number. In [6, 7] a potential for the dilaton field is constructed to reproduce some key features of Yang-Mills theory in 4 dimensions, namely heavy quark confinement in the infrared and asymptotic freedom in the ultraviolet. Recently, a variant of this construction was suggested in [8] whereby the dilaton field is directly tied to the running of the gauge coupling in the Yang-Mills theory. This construction is more transparent physically as it directly ties the holographic direction to the running of the gauge coupling constant. It is also less numerically intensive. We follow [8] and add a U(1) charge field in bulk to account for the effects of a finite chemical potential at the boundary.

In section 2 we discuss the bottom-up improved holographic model in 5 dimensions with bulk gravity coupled to a dilaton and the U(1) charged field. The dilaton dynamics follows from the running of the gauge coupling. The dilaton potential is fixed by the equations of motion. Explicit solutions are constructed in section 3. In section 4 we discuss the small and big charged black hole solutions, and their ensuing bulk thermodynamics. In section 5 we analyze the fermionic susceptibilities and compare them to the ideal gas limit. In section 6, the Polyakov line is evaluated at finite temperature and chemical potential. In section 7 we discuss the role of the chemical potential on the spatial and temporal string tension. Our conclusions are in section 8. The sensitivity of the model to the dilaton-gauge-field coupling is discussed in Appendix A. In Appendix B we derive (quark) susceptibilities for a warped holographic model without a dilaton.

2 The Model

In the Einstein frame the 5-dimensional Einstein-Maxwell action in the background of a scalar or dilaton field ϕ, is given by [6, 7]

$$S = \frac{1}{16\pi G_5}\left(\int d^5x\sqrt{-g}\left(R - \frac{4}{3}\partial_A\phi\partial^A\phi + V(\phi) - \frac{\mathfrak{L}^2}{4}e^{c\phi}F_{AB}F^{AB}\right) - 2\int d^4x\sqrt{h}K\right) \quad (1)$$

with the $U(1)$ gauge field tensor $F_{AB} = \partial_{[A}A_{B]}$ and $\mathfrak{L}$ the radius of the AdS-space in the conformal limit. The Gibbons-Hawking boundary term gives no contribution to the equations of motion but is crucial for evaluating the on-shell action [9]. The coupling to the $U(1)$ charge is a generalization of [10], where we consider the parameter c in the exponential gauge coupling as a free parameter. A recent analysis in this direction is found in [11]. For a non-constant scalar field $\phi = \phi(z)$ the Bianchi identity $\nabla^A G_{AB} = 0$ (with G_{AB} the Einstein tensor) ensures that the Einstein equations imply the equation of motion for the scalar field. With the following Ansatz for the metric

$$ds^2 = b(z)^2\left(-f(z)dt^2 + d\vec{x}^2 + \frac{1}{f(z)}dz^2\right) \quad (2)$$

we follow [6, 7, 8] and assume that the β-function for the gauge field theory on the boundary at $z = 0$ is given by

$$\beta(\lambda) = b\frac{d\lambda}{db} = -\beta_0\lambda^q \quad (3)$$

with the running t'Hooft coupling $\lambda(z) = e^{\phi(z)} \sim g_{YM}^2 N_c$. Note that (3) does not follow from varying the action (1). $q \geq 1$ ensures confinement in the IR and the values $q = 10/3$ and

$\beta_0 = 488.8$ have been shown in [12] to reproduce the dilaton potential in [13] to lowest order in λ. We will use these values in our numerical analysis. For a static, charged black hole solution the equation of motion for the scalar potential $A_0(z)$ is given by

$$\begin{aligned} b(z)^{-5}\partial_z\left(b(z)e^{c\phi(z)}A_0'(z)\right) &\propto \delta(z - z_{charge}) \\ A_0'(z) &= -\frac{\mathbf{e}}{\mathcal{L}^3}\frac{e^{-c\phi(z)}}{b(z)} \end{aligned} \tag{4}$$

with $A_0'(z) = \frac{\partial}{\partial z}A_0(z)$ and the electric charge $\mathbf{e}$ located at some position z_{charge} behind the horizon of the black hole. We can now solve the Einstein equations

$$6\frac{b'^2}{b^2} - 3\frac{b''}{b} - \frac{4}{3}\phi'^2 = 0 \tag{5}$$

$$\frac{3}{2}\frac{b'f'}{b} + \frac{1}{2}f'' - \frac{\mathcal{L}^2 e^{c\phi}}{2b^2}A_0'^2 = 0 \tag{6}$$

$$\frac{9}{2}\frac{b'f'}{bf} + 3\frac{b''}{b} + 6\frac{b'^2}{b^2} + \frac{1}{2}\frac{f''}{f} - \frac{b^2}{f}V = 0 \tag{7}$$

together with (3) and (4). Note that the factor $f(z)$ drops out from the spatial components of the energy-momentum tensor for the gauge field.

3 Solutions

The solution for the electrostatic potential is given by

$$A_0(z) = -\frac{\mathbf{e}}{\mathcal{L}^3}\int_0^z dx\frac{e^{-c\phi(x)}}{b(x)} + \mu \ . \tag{8}$$

The integration constant μ is interpreted as the chemical potential since $A_0(z \to 0) = \mu$ [14]. The requirement for the electrostatic potential to vanish at the horizon of the black hole, see (23), gives

$$A_0(z_H) = 0 \Leftrightarrow \mu = \frac{\mathbf{e}}{\mathcal{L}^3}\int_0^{z_H} dx\frac{e^{-c\phi(x)}}{b(x)} \ . \tag{9}$$

The warping factor $b(z)$ is not influenced by the presence of the charge and the solution to (3) is given by

$$Q = \ln\frac{b}{b_0} = \frac{1}{(q-1)\beta_0}\frac{1}{\lambda^{q-1}} \ . \tag{10}$$

Since

$$W(\lambda) = \frac{-b'(z)}{b(z)^2} = W(0)e^{\frac{a}{4Q}} \tag{11}$$

and $a=\left(\frac{4}{3(1-q)}\right)^2$, (5) yields

$$z=\frac{\mathcal{L}}{b_0}\int_Q^\infty dx\ e^{-x-\frac{a}{4x}}\ , \tag{12}$$

where the constant $1/W(0)=\mathcal{L}$ is fixed by the boundary value of the potential $V(z)$, see (22) and [8]. (10) and (12) imply that neither the warping $b(z)$, nor the coupling λ depend on the temperature or chemical potential. (12) introduces a scale $\Lambda=\frac{b_0}{\mathcal{L}}$ for our model and implies an upper bound on the radial coordinate

$$z\le\frac{\mathcal{L}}{b_0}\int_0^\infty dxe^{-x-\frac{a}{4x}}=z_w\ . \tag{13}$$

A static wall in the IR is generated which leads to an area law for the Polyakov loop as we will detail below.

Expanding the integral in (12) for small z (large Q)

$$\int_Q^\infty dxe^{-x-\frac{a}{4x}} = \sum_0^\infty\frac{1}{n!}\left(-\frac{a}{4}\right)^n\Gamma(1-n,Q) \tag{14}$$

$$= \exp\left[-Q-\frac{a}{4Q}\right]\left(1+\frac{a}{4Q^2}-\frac{a}{2Q^3}\ +\ ...\right) \tag{15}$$

with the incomplete Gamma-function $\Gamma(1-n,Q)$ we obtain $b(z\to 0)=\frac{\mathcal{L}}{z}$ and $\phi(z\to 0)\propto-\log\left(-\log\Lambda z\right)$, which reproduces a logarithmic running coupling for the model on the boundary.

Changing variables from z to Q in (6) reads

$$\partial_Q^2 f(Q)+\left(-\frac{a}{4Q^2}+4\right)\partial_Q f(Q)=\frac{((q-1)\beta_0)^{\frac{c}{q-1}}\mathbf{e}^2}{\mathcal{L}^2b_0^6}e^{\frac{-a}{2Q}-6Q}Q^{\frac{c}{q-1}}\ . \tag{16}$$

The two asymptotic conditions on $f(z)$, $f(z=0)=f(Q=\infty)=1$ and $f(Q_H)=0$ at the horizon $Q_H=Q(z_H)$, fix the two integration constants and we obtain

$$f(Q)=1+C_1i(Q)+\delta\frac{(\mu/\Lambda)^2}{j(Q_H)^2}\int_\infty^Q dx\ e^{-\frac{a}{4x}-4x}\int_\infty^x dy\ e^{-\frac{a}{4y}-2y}y^{\frac{c}{q-1}} \tag{17}$$

with $\delta=\frac{1}{((q-1)\beta_0)^{\frac{3c}{1-q}}}$ and

$$C_1 = \frac{-1-\delta\frac{(\mu/\Lambda)^2}{j(Q_H)^2}\int_\infty^{Q_H}dx\ e^{-\frac{a}{4x}-4x}\int_\infty^x dy\ e^{-\frac{a}{4y}-2y}y^{\frac{c}{q-1}}}{i(Q_H)} \tag{18}$$

$$j(Q) = \int_\infty^Q dx\ e^{-\frac{a}{4x}-2x}x^{\frac{c}{1-q}} \tag{19}$$

$$i(Q) = \int_\infty^Q dx\ e^{-\frac{a}{4x}-4x}. \tag{20}$$

We see that our solutions for $f(z)$ reduces to the one obtained in [8] for $\mu = 0$. With a vanishing coupling of the dilaton to the gauge field, i.e. $c = 0$, the metric in the Einstein frame (2) approaches the RN-AdS-metric for $z \to 0$ with

$$f(z \to 0) \to 1 - \frac{C_1}{4}(\Lambda z)^4 + \frac{(\mu/\Lambda)^2}{24 j(Q_H)^2}(\Lambda z)^6 \ . \tag{21}$$

We can now solve (7) for the scalar potential

$$V(Q) = W(0)^2 e^{\frac{a}{2Q}} \Big(\frac{1}{2}\partial_Q^2 + \big(5 - \frac{a}{8Q^2}\big)\partial_Q + 12 - \frac{3a}{4Q^2}\Big) f(Q) \tag{22}$$

As ϕ is temperature independent this implies $V(Q) = V(\phi, T, \mu)$. The dependence on temperature and chemical potential follows from $f(Q)$. The normalization $V(z \to 0) = V(Q \to \infty) = \frac{12}{\mathfrak{L}^2}$ gives $\frac{1}{W(0)} = \mathfrak{L}$.

4 Thermodynamics

The Hawking temperature of the black hole,

$$T = \frac{1}{4\pi} f'(z_H) \ , \tag{23}$$

is given by

$$T = \frac{-\Lambda}{4\pi} \frac{e^{-3Q_H}}{i(Q_H)} \left(1 - \delta(\mu/\Lambda)^2 \frac{k(Q_H)}{j(Q_H)^2}\right) \tag{24}$$

with $z_H, Q_H = Q(z_H)$ the position of the horizon and

$$k(Q) = \int_\infty^Q dx e^{-\frac{a}{4x} - 4x} \int_x^Q dy e^{-\frac{a}{4y} - 2y} y^{\frac{c}{q-1}} . \tag{25}$$

At vanishing chemical potential the black hole solution has a minimal non-zero temperature. The two regions $T'(z_H) > 0$ ($T'(Q_H) < 0$) and $T'(z_H) < 0$ ($T'(Q_H) > 0$) correspond to a small and a big black hole branch. Since the solution for $\mu = 0$ shows a minimum temperature, a certain density ($\mu_0 = 2.8\Lambda$) is needed to obtain a solution with zero temperature. Here, we will focus on the case of vanishing dilaton-gauge-field coupling, i.e. $c = 0$, and consider the case $c = 4$ separately in Appendix A. For $T \to 0$ and $\mu \geq \mu_0$, the small black hole vanishes leaving only the big black hole solution, see Fig. 1, and the metric in the IR becomes $\mathrm{AdS}_2 \times \mathbb{R}^3$, [15, 16]. With $(z - z_H) = \gamma/\zeta$, $t = 2/(\gamma f''(z_H))\tau$ and $\gamma \to 0$, ζ, τ finite, (2) reduces to

$$ds^2 = \left(\frac{2b(z_H)^2}{f''(z_H)}\right) \frac{1}{\zeta^2} \left(-d\tau^2 + d\zeta^2\right) + b(z_H)^2 d\vec{x}^2 \ . \tag{26}$$

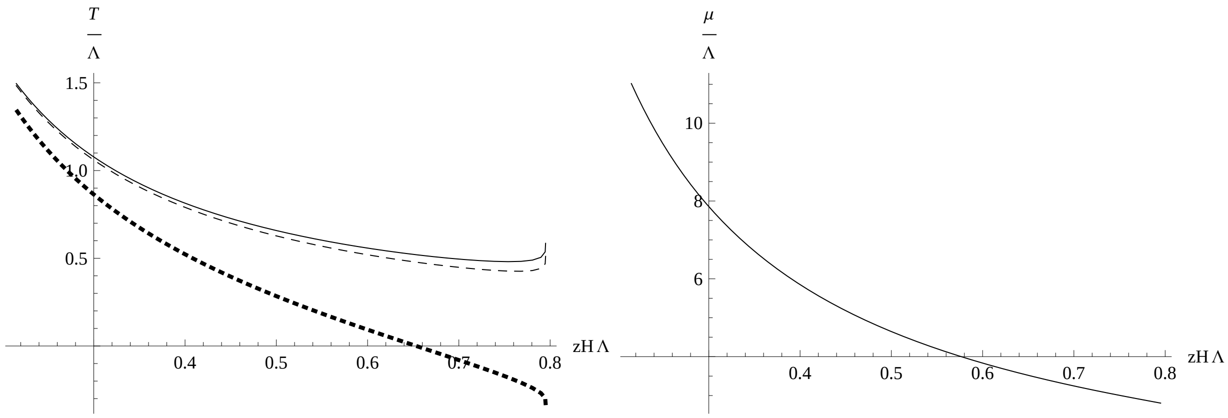

Figure 1: Left: The Hawking temperature at chemical potentials $\mu/\Lambda = 0$ (solid), 1 (dashed), 3.5 (dotted) as a function of the scaled horizon $z_H\Lambda$. Right: The chemical potential at $T = 0$. $(c = 0)$

One crucial step in the above analysis is that the temperature as a function of the horizon does not have a minimum as $T \to 0$, i.e. $f''\left(z_H(T = 0, \mu)\right) \neq 0$. In our case this translates to the disappearance of the small black hole as $T \to 0$.

Note that regularizing the action in (1) by subtracting a 'vacuum' (thermal gas) solution with functions $\phi_0, b_0, f_0 = 1$ does not necessarily yield the grand potential since the scalar potential (22) has additional temperature and chemical potential dependence thereby upsetting the Gibbs relations. This notwithstanding, we can still define the entropy density $s(T, \mu)$ carried by the black hole through its area as

$$s(T, \mu) = \frac{b_0^3}{4G_5} e^{3Q_H}. \tag{27}$$

The small (big) black hole branches have negative (positive) specific heat, $c_v \propto T ds/dT$, and are unstable (stable).

The scaled entropy density s/T^3 reaches its asymptotic value around $T \simeq 2T_0$ and develops a peak with increasing μ. A low temperature and high density expansion yields

$$s(\mu \gg T) = \frac{b_0^3}{4G_5} \left(\frac{1}{6\sqrt{6}} \frac{\mu^3}{\Lambda^3} + \frac{\pi}{4} \frac{\mu^2 T}{\Lambda^3} + \frac{\pi^2 3\sqrt{3}}{8\sqrt{2}} \frac{\mu T^2}{\Lambda^3} + \frac{a\pi\sqrt{3}}{16\sqrt{2}} \frac{\mu T^2}{\Lambda^3 \log \frac{\mu}{\Lambda\sqrt{6}}} + \mathcal{O}(T/\mu) \right). \tag{28}$$

(28) reduces to the RN-AdS entropy [17] up to logarithmic corrections. Much like the RN-AdS black hole, our black hole solution carries a finite entropy at zero temperature and a linear specific heat, see Fig. 4. The effects of the running coupling through the scalar field causes only logarithmic corrections much like the high temperature case.

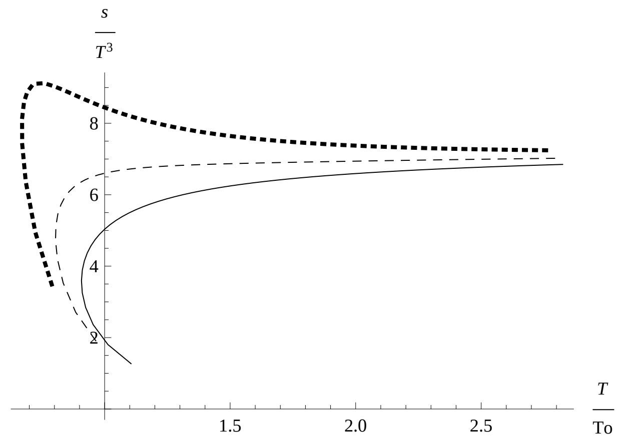

Figure 2: The scaled entropy density s/T^3 at chemical potentials $\mu/\Lambda = 0$ (solid), 1 (dashed), 1.5 (dotted) with $T_0 = 170\text{MeV}$ and $\Lambda = 321\text{MeV}$. Both the contributions from the small and big black hole are shown.

The pressure at vanishing chemical potential is obtained by integrating the entropy density over the small and big black hole branch

$$p(T, \mu = 0) = \int_0^{Q_H(T,\mu=0)} dQ \left(\frac{\partial T}{\partial Q}\right) s(Q(T, \mu = 0)). \tag{29}$$

The scale $\Lambda = \frac{b_0}{\mathcal{L}}$ is fixed by requiring that the pressure at $\mu = 0$ vanishes at a critical temperature $T_0 = 170\text{MeV}$ or $\Lambda = 321\text{MeV}$. Comparison with an ideal gluon gas gives $\frac{b_0^3}{G_5} = \frac{16N_c^2\Lambda^3}{45\pi}$ [8].

The pressure of the small black hole is negative, indicating its instability. Fig. 3 shows the big black hole contribution to the pressure. For $T/T_0 < 1$ the 'vacuum' solution dominates. The integration constant in (29) is fixed by analyzing the high temperature thermodynamics of the small black hole, [9]. Since the small black hole vanishes for $T = 0$, we fix the integration constant by setting the zero temperature pressure to zero at $\mu_0 = \mu_{min}\Big|_{T=0} = \mu\,(T = 0, Q_H = 0) = 2.8\Lambda$,

$$p(T = 0, \mu) = \int_0^{Q_H(T=0,\mu)} dQ \left(\frac{\partial \mu}{\partial Q}\right) n(Q(T = 0, \mu)), \tag{30}$$

with the charge density n given by (31). Fig. 3 shows that the black hole solution is unstable against the vacuum solution below μ_0. In contrast, the RN-AdS black hole at zero temperature [18], dominates the action for all chemical potentials down to $\mu = 0$.

For fixed chemical potential the charge density $n(T, \mu)$ is proportional to the electric

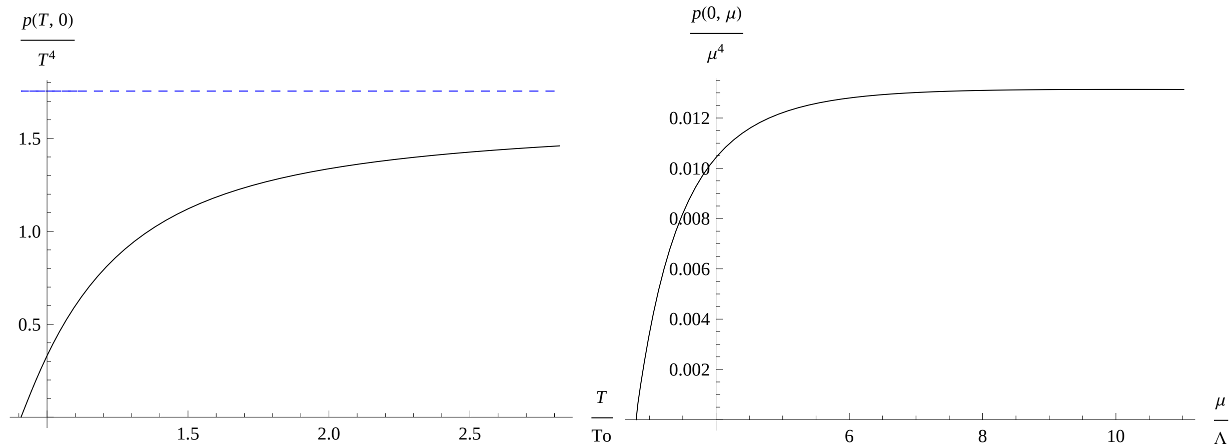

Figure 3: Left: Big black hole pressure at $\mu = 0$ ($N_c = 3$) and pressure of an ideal gluon gas $P_{ideal\ gas}/T^4 = 2\,(N_c^2 - 1)\,\frac{\pi^2}{90}$ (dashed). Right: Pressure at $T = 0$ ($N_c = N_f = 3$). For an ideal relativistic Fermi gas of N_f massless quark flavors $P_{ideal\ gas}/\mu^4 = \frac{N_f}{4\pi^2}$.

charge $\mathbf{e}$ and using (9) we write

$$n = \frac{\alpha}{b_0^4}\mathbf{e} = \frac{\alpha \mathcal{L}^3 \mu}{b_0^4 \int_0^{z_H} dx \frac{e^{-c\phi(x)}}{b(x)}} = \frac{-\alpha \delta^{-1/3}\mu}{\Lambda^2 m(Q_H)} \tag{31}$$

with the proportionality constant α and

$$m(Q) = \int_\infty^Q dx Exp\left(-\frac{a}{4x} - 2x\right) x^{\frac{c}{q-1}} \ . \tag{32}$$

For $\mu \gg T$ we obtain

$$n(\mu \gg T) = \frac{2\alpha}{\Lambda}\left(\frac{1}{6}\frac{\mu^3}{\Lambda^3}(1 + \frac{a}{4\log\frac{\mu}{\Lambda\sqrt{6}}}) + \frac{\mu^2 T}{\Lambda^3}(\frac{\pi}{\sqrt{6}} + \frac{a\pi(3+\sqrt{6})}{24\log\frac{\mu}{\Lambda\sqrt{6}}}) + \mathcal{O}(T/\mu)\right). \tag{33}$$

As in the RN-AdS, the leading order low temperature correction is linear in T. The deviation from the pure RN-AdS shows up as logarithmic corrections.

5 Susceptibilities

In QCD at low density and high temperature the pressure can be expanded as

$$\frac{p(T,\mu)}{T^4} = \sum_{n=0}^{\infty} c_n(T)\left(\frac{\mu}{T}\right)^n \tag{34}$$

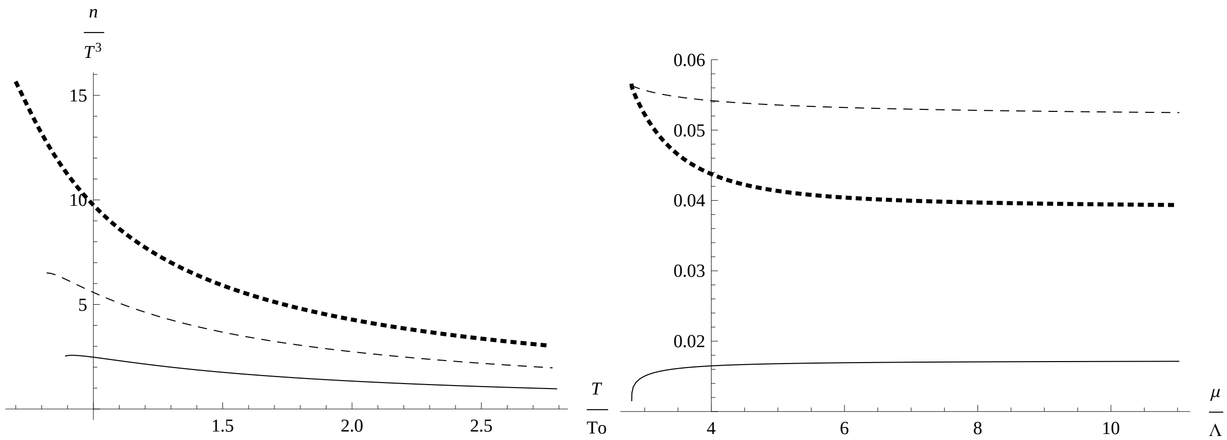

Figure 4: Left: Scaled charge density n/T^3 for the big black hole at densities $\mu/\Lambda = 0.5$ (solid), 1 (dashed), 1.5 (dotted) with $\alpha = \frac{3}{2\pi^2}\Lambda^4$. Right: s/μ^3 (solid), n/μ^3 (dashed), e/μ^4 (dotted) at $T = 0$.

with the (flavor symmetric) quark susceptibilities

$$c_n(T) = \frac{1}{n!}\frac{\partial^n}{\partial(\frac{\mu}{T})^n}\frac{p(T,\mu)}{T^4}\Big|_{\mu=0}. \tag{35}$$

Various hadronic susceptibilities in the transition region around $T_0 = 170$MeV at vanishing quark chemical potential show distinct characteristics. In particular, lattice studies [19] and expectations from PNJL models [20] both confirm that c_4, c_6 show distinct peaks at a critical temperature T_c. Asymptotics of the susceptibilities come close to the ideal gas values at temperatures $T \simeq 2T_c$. These charge density fluctuations are obtained as derivatives with respect to the density on the grand canonical partition function.

The quark number susceptibility in hard and soft wall AdS/QCD models were studied in [21, 22]. In these models the first non-vanishing coefficient in the expansion (34) show a jump at a critical temperature due to a Hawking-Page transition. In the improved model under consideration with running gauge coupling, we can explicitly assess the first few moments in (34). We first note that the odd moments vanish since $m(Q_H)$ in (31) receives corrections at high T (high Q_H) of the form μ^2/T^2. From (31) we obtain

$$\begin{aligned} c_2(T) &= \frac{1}{2T^2}\frac{\partial}{\partial\mu}n(T,\mu)\Big|_{\mu=0} && (36)\\ &= \frac{-\alpha\delta^{-1/3}}{2T^2\Lambda^2}\frac{1}{m(Q_H)}\Big|_{\mu=0}. && (37)\end{aligned}$$

Note that eqn. (23) implies

$$\left(\frac{\partial Q_H}{\partial\mu}\right)\Big|_{\mu=0} = 0\ , \tag{38}$$

$$\left(\frac{\partial^2 Q_H}{\partial \mu^2}\right)\Big|_{\mu=0} = \frac{\delta}{2\pi\Lambda T}\frac{Exp\left(-3Q_H\right)}{\left[3i(Q_H)+Exp(-4Q_H-\frac{a}{4Q_H})\right]}\frac{k(Q_H)}{(j(Q_H))^2}\Big|_{\mu=0}, \quad (39)$$

$$\left(\frac{\partial^4 Q_H}{\partial \mu^4}\right)\Big|_{\mu=0} = -3\left(\frac{\partial^2 Q_H}{\partial \mu^2}\right)^2\left(\frac{\partial^2 T}{\partial Q_H^2}\right)\left(\frac{\partial Q_H}{\partial T}\right)\Big|_{\mu=0}. \quad (40)$$

We obtain for $c_4(T), c_6(T)$

$$c_4(T) = \frac{1}{24}\frac{\partial^3}{\partial\mu^3}n(T,\mu)\Big|_{\mu=0} \quad (41)$$

$$= \frac{-\alpha\delta^{-1/3}}{24\Lambda^2}\left(\frac{\partial^2 Q_H}{\partial\mu^2}\right)\frac{\partial}{\partial Q_H}\frac{1}{m(Q_H)}\Big|_{\mu=0} \quad (42)$$

$$c_6(T) = \frac{T^2}{6!}\frac{\partial^5}{\partial\mu^5}n(T,\mu)\Big|_{\mu=0} \quad (43)$$

$$= \frac{-\alpha\delta^{-1/3}T^2}{6!\Lambda^2}\left(\left(\frac{\partial^4 Q_H}{\partial\mu^4}\right)\frac{\partial}{\partial Q_H}+3\left(\frac{\partial^2 Q_H}{\partial\mu^2}\right)^2\frac{\partial^2}{\partial Q_H^2}\right)\frac{1}{m(Q_H)}\Big|_{\mu=0}. \quad (44)$$

As can be seen from a high temperature expansion of the integrals in (37), (44) ($Q_H \to \infty$) c_4 and c_6 do not converge to a finite asymptotic high temperature value *unless* $c = 0$. Thus, a meaningful comparison to QCD demands a vanishing coupling of the dilaton ϕ to the $U(1)$ charge. With $c = 0$ the high temperature asymptotics are given by

$$c_2 \to \pi^2\left(\frac{\alpha}{\Lambda^4}\right) \quad (45)$$

$$c_4 \to \frac{1}{18}\left(\frac{\alpha}{\Lambda^4}\right) \quad (46)$$

$$c_6 \to \frac{1}{540\pi^2}\left(\frac{\alpha}{\Lambda^4}\right). \quad (47)$$

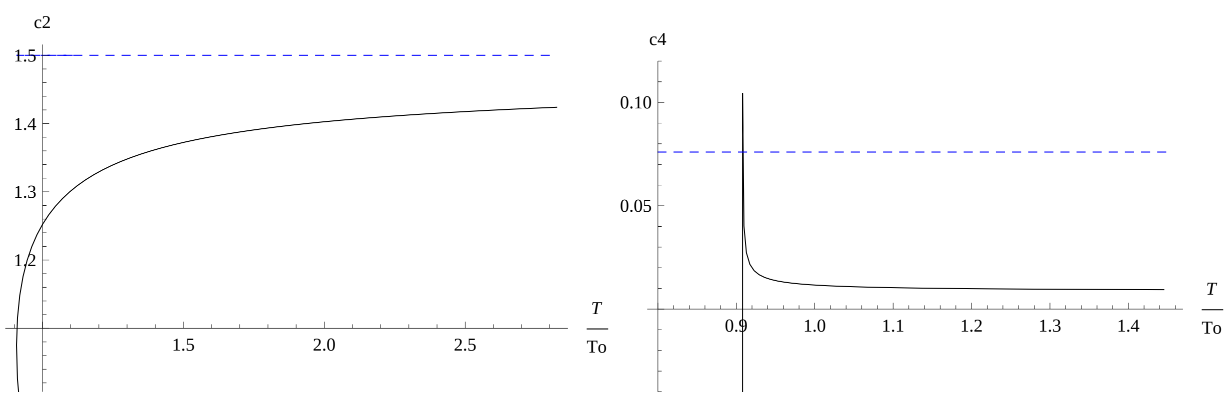

Figure 5: Susceptibilities for the big black hole. Dashed line: ideas gas value for $N_c = N_f = 3$.

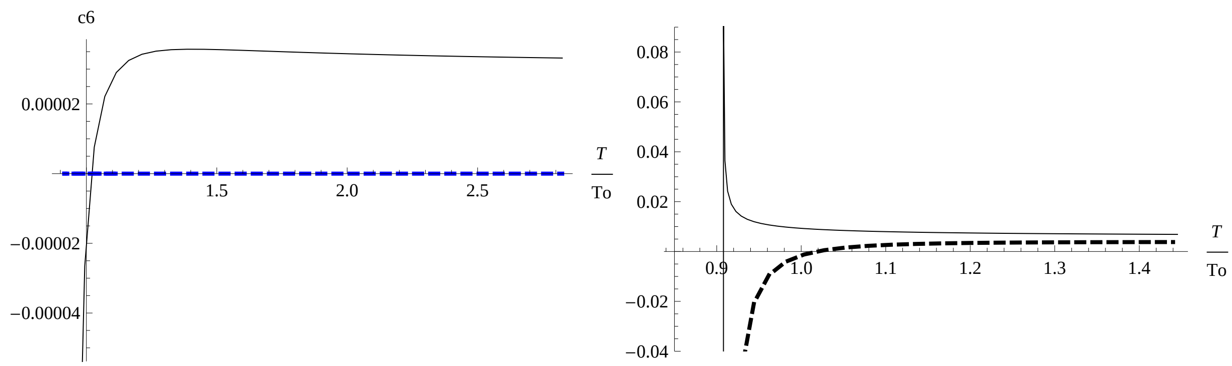

Figure 6: Left: c_6 and ideal gas value for $N_c = N_f = 3$ (dashed). Right: Ratios c_4/c_2 (solid) and c_6/c_4 (dashed)

As a result of the non-trivial warping $b(z)$, the susceptibilities are non-constant and a comparison with recent lattice data [19] shows that the susceptibilities c_2, c_4, c_6 obtained in this model have the correct shape around the critical temperature T_0. c_2 and c_6 approach its asymptotic value from below, while c_4 shows a distinct peak at the critical temperature. All high temperature asymptotics of the susceptibilities are strictly positive. For the model proposed in [23], the susceptibilities vanish as explained in Appendix B.

In comparison, for an ideal gas of massless quarks and anti-quarks the susceptibilities read $c_2^{ideal\ gas} = \frac{N_c N_f}{6}$, $c_4^{ideal\ gas} = \frac{N_c N_f}{12\pi^2}$, $c_6^{ideal\ gas} = 0$ with the ratios $c_4^{ideal\ gas}/c_2^{ideal\ gas} = 1/(2\pi^2)$, $c_6/c_4 = 0$. In our model: $c_4/c_2 = 1/(18\pi^2)$, $c_6/c_4 = 1/(30\pi^2)$. While the scale Λ was fixed by the gluonic part of the pressure, we fix the constant α by comparing to the fermionic part of the pressure of an ideal gas. For $N_c = 3$, $N_f = 3$ we fit the high temperature asymptotic of c_2 to the ideal gas value and obtain $\alpha = \frac{3}{2\pi^2}\Lambda^4$. The susceptibilities in the holographic model considered in [17] with a non-confining RN-AdS black hole are constant and given by $c_2^{RN-AdS} = N_c^2\gamma^2/8$, $c_4^{RN-AdS} = \frac{N_c^2\gamma^4}{48\pi^2}$, $c_6^{RN-AdS} = -\frac{N_c^2\gamma^6}{216\pi^4}$, where the flavor dependence is embedded in the parameter $\gamma^2 \propto N_f/N_c$.

It is now straightforward to evaluate the density contribution to the pressure, $\Delta p(T, \mu \neq 0)/T^4 = \sum_{n=2}^{\infty} c_n(T)\left(\frac{\mu}{T}\right)^n \simeq c_2(T)\left(\frac{\mu}{T}\right)^2 + c_4(T)\left(\frac{\mu}{T}\right)^4 + c_6(T)\left(\frac{\mu}{T}\right)^6$, and the energy density $e(T, \mu) = Ts - p + \mu n$ at high temperatures and small charge density. Fig. 7 shows our results for $(e - 3p)/T^4$ at different densities.

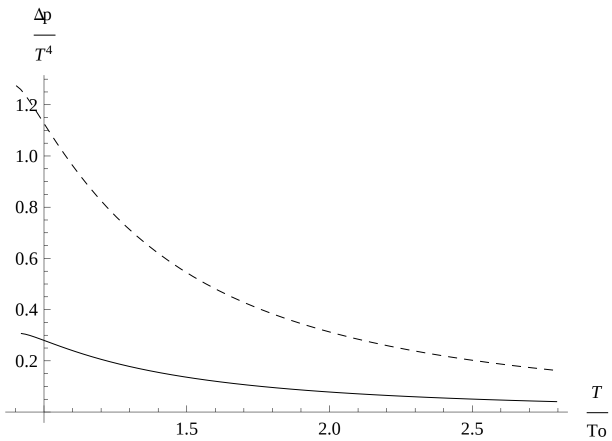

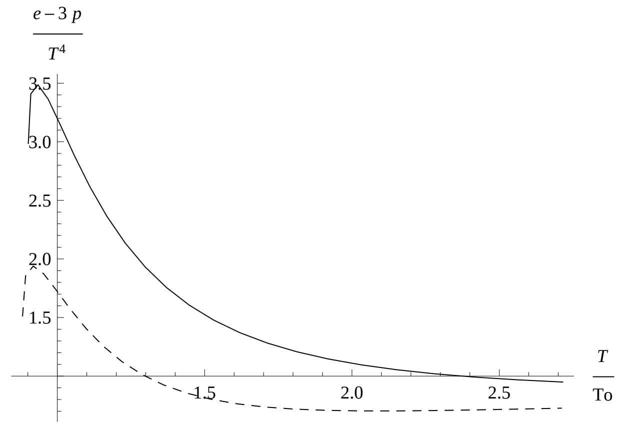

Figure 7: $\Delta p/T^4$ and $(e-3p)/T^4$ for $\mu/\Lambda = 0.25$ (solid), 0.5 (dashed).

6 Polyakov line

The expectation value of the Polyakov line can be schematically written as [24, 25]

$$\langle L(T,\mu)\rangle = \sum_n w_n Exp(-S_n) \ , \tag{48}$$

with weights w_n associated with a renormalized area S_n. We will approximate the area using the Nambu-Goto action describing a fundamental string stretched between the horizon and the boundary at $z=0$. While on-shell quantities such as the susceptibilities do not depend on the frame, quantities such as the Polyakov line may depend on it. The appropriate background for the string is given by the metric in the string frame

$$g^s_{AB}(z) = e^{\frac{4}{3}\phi(z)} g_{AB}(z) \ , \tag{49}$$

where g_{AB} is given in eqn. (2). For a static configuration with the parametrization $\xi_1 = t$, $\xi_2 = z$ the action is given by

$$\begin{aligned} S_{NG} &= \frac{1}{2\pi\alpha'}\int d^2\xi \sqrt{g^s_{AB}\partial_M X^A \partial_N X^N} & (50)\\ &= \frac{1}{2\pi\alpha' T}\int_0^{z_H} dz b(z)^2 \lambda(z)^{\frac{4}{3}}\sqrt{1+f(z)\vec{x}\,'(z)^2}. & (51)\end{aligned}$$

The first integral gives the equation of motion for $\vec{x}(z)$

$$\frac{d}{dz}\left(\frac{b(z)^2\lambda(z)^{\frac{4}{3}} f(z)\vec{x}\,'(z)}{\sqrt{1+f(z)\vec{x}\,'(z)^2}}\right) = 0. \tag{52}$$

It is easy to check that the dominant contribution to the integral in (51) comes from the solution $\vec{x} = const.$, and we will neglect other solutions. Since our metric is asymptotically

RN-AdS, implying that $b(z \to 0) = \frac{\mathcal{L}}{z}$, the action defined in (51) is divergent. We renormalize the action by subtracting the vacuum contribution stretching from the boundary ($z = 0$) upto the wall at z_w. The Polyakov line in the saddle-point approximation (48) reads

$$\begin{aligned}
\langle L(T,\mu)\rangle &\simeq w_0 Exp\left(-S_{NG}^{ren}\right) && (53)\\
&= w_0 Exp\left(\frac{1}{2\pi\alpha' T}\int_0^{z_H} dz b(z)^2 \lambda(z)^{\frac{4}{3}} - \frac{1}{2\pi\alpha' T}\int_0^{z_w} dz b(z)^2 \lambda(z)^{\frac{4}{3}}\right) && (54)\\
&= w_0 Exp\left(\frac{1}{2\pi\alpha' T}\int_{z_w}^{z_H} dz b(z)^2 \lambda(z)^{\frac{4}{3}}\right). && (55)
\end{aligned}$$

At vanishing chemical potential, the 'low' temperature limit of the Polyakov line is given by

$$\langle L(T \to T_{min}, 0)\rangle \propto Exp\Big[Exp\left(-\frac{1}{Ln(T/T_{min})}\right)\left(\frac{1}{Ln(T/T_{min})}\right)^{\frac{4}{3(q-1)}}\Big] \qquad (56)$$

and, thus, shows little deviation from its high temperature asymptotic value. Fig. 8 shows the behavior of the approximate order parameter of the phase transition. The constant b_0^2/α' is fixed by comparing the spatial string tension with lattice data, see next section. At fixed μ the expectation value of the Polyakov line jumps rapidly from a minimum value at a temperature $T = T_{min}$ and approaches a constant value in the high temperature region. A direct comparison with lattice data is unfortunately not possible given the subtraction dependence inherent in the definition of the Polyakov line both on the lattice and in our case. This point is generally overlooked in most analyses.

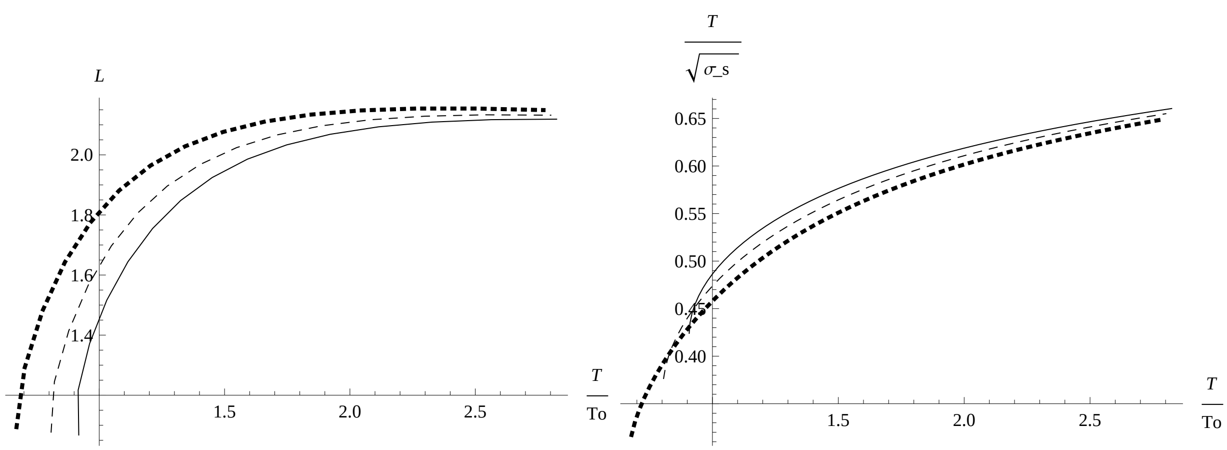

Figure 8: Left: Polyakov line with $\mu/\Lambda = 0$ (solid), 1 (dashed), 1.5 (dotted); ($w_0 = 1$). Right: Big black hole contribution to the spatial string tension at densities $\mu/\Lambda = 0$ (solid), 1.5 (dashed), 2.5 (dotted).

7 String tensions

The analyses of the spatial and temporal (effective) string tension, σ_s and σ at finite temperature and density, are identical to those carried in [12] at finite temperature. Indeed, a rerun of their analysis shows that for the spatial string tension σ_s, the density dependence is entirely encoded in the position of the horizon $z_H(T,\mu)$ with

$$\sigma_s(T,\mu) = \frac{1}{2\pi\alpha'} b_s(z)^2\Big|_{z=z_H} = \frac{1}{2\pi\alpha'} b(z)^2 \lambda(z)^{\frac{4}{3}}\Big|_{z=z_H}, \tag{57}$$

where $b_s(z)$ is the warping in the string frame. A comparison with lattice data [26] at $T = T_0$, $\mu = 0$ fixes $\frac{b_0}{\sqrt{\alpha'}} = 3 * 10^{-4}\text{MeV}^{-1}$. For chemical potentials up to $\mu = 2.5\Lambda$, the spatial string tension shows a weak dependence on the chemical potential in this improved holographic model.

In the temporal Wilson loop, the string tying a heavy quark and antiquark in the bifundamental representations extends in the holographic direction in bulk. The further the spatial separation L, the deeper the string extends in bulk z. Specifically [12]

$$L(z^*) = 2\int_0^{z^*} dz \frac{1}{\sqrt{f(z)\left(\frac{b_s^4(z)f(z)}{b_s(z^*)f(z^*)} - 1\right)}} \tag{58}$$

with z^* the maximum holographic depth for the pending string. In the black hole background with $f \neq 1$, $L(z^*)$ is finite for any temperature and chemical potential as shown in Fig. 9.

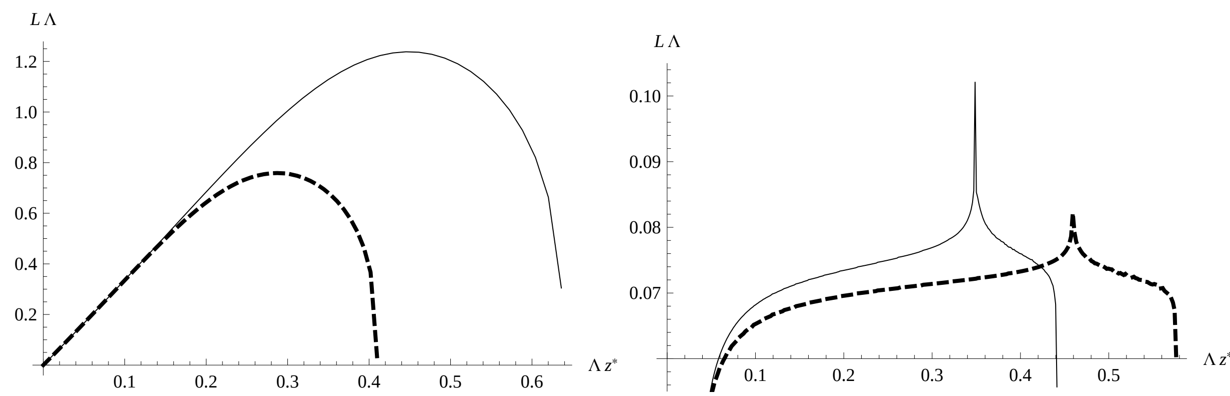

Figure 9: Length separating two heavy quarks. Left: $\mu = 0$ with $T = T_0$ (solid) and $T = 1.5T_0$ (dashed). Right: $T = T_0, \mu = \mu_0 = 2.8\Lambda$ (solid) and $T = 0, \mu = 4\Lambda$ (dashed).

In the black hole background two heavy-quarks still tie up to distances of order L_{max} which is the location of the maximum in Fig. 9. In other words, for $0 < L < L_{max}$ we expect a linear-like free energy between two heavy quarks, while for $L > L_{max}$ the heavy quarks "screen" through the large entropy of the string (at zero density) or through fundamental matter (at finite density) causing the free energy to plateau at twice the screening masses. Around the phase transition points, $T = T_0$ and $\mu = 0$, $L_{max} = 1.24\Lambda^{-1} \approx 0.76\, fm$, while for $T = 0$ and $\mu = \mu_0 = 2.8\Lambda$, $L_{max} = 0.10\Lambda^{-1} \approx 0.06\, fm$. The larger the density, the larger the screening.

8 Conclusions

Finite density QCD both at zero and finite temperature is still a challenging problem from first principles. In the double limit of a large number of colors and large t'Hooft coupling the holographic approach offers a non-perturbative tool for investigating QCD-like gauge theories at finite temperature and density. The current analysis provides a step in that direction whereby finite density effects are incorporated in an improved AdS/QCD model with a bulk U(1) charge. Without a dilaton-gauge coupling, our improved AdS/QCD metric at finite (charge) density is asymptotically RN-AdS on the boundary with a non-trivial dilaton profile interpreted as a running coupling. The effects of the density do not alter the warping factor of the underlying gravitational metric.

At zero density but for temperatures larger than a minimum temperature, the gravitational equations yield a pair of black holes of different holographic sizes. A small black hole that is unstable thermodynamically, and a large black hole that is stable. The occurence of a minimum temperature in the improved model reflects on the (first order) transition from a 'vacuum' (thermal gas) to a black hole solution. The unstable solution is found to disappear at large densities. For zero temperature, the small black hole solution disappears while the large black hole solution requires a minimum chemical potential $\mu_0 = 2.8\Lambda$. As a result, the metric becomes $\mathrm{AdS}_2 \times \mathbb{R}^3$ in the infrared. Evaluating the pressure at finite μ and $T = 0$ shows that the 'vacuum' becomes unstable against black hole solution at a critical $\mu = \mu_0$ indicating a first order Hawking-Page transition.

The (quark) susceptibilities $c_2,\ c_4,\ c_6$ show rapid variations across the critical temperature T_0 in the improved holographic model, in contrast to the RN-AdS model where they are found to be constant. The variations are overall consistent with the ones reported by lattice simulations. However, their asymptotic ratios are off compared to the free fermion (quark) limits, despite the fact that in the improved holographic model the gauge coupling on the boundary runs weak at high temperature.

To further clarify the nature of the charged black hole solutions, we have analyzed the subtracted Polyakov line and found that it jumps at both finite temperature and/or finite density. The jump is suggestive of screening which is expected to be larger at finite charge density. Indeed, our analysis of the temporal Wilson loop confims that two heavy quarks detach more easily at higher density. Spatial Wilson loops are midly affected by the charge screening in the black-hole background.

The bottom-up model with running coupling constant appears to capture some essentials of a first order transition from a vacuum with matter characterized by $f = 1$ and a charged black-hole characterized by $f \neq 1$. This first order geometrical transition captured by the holographic gravity equations appears to encode some of the features expected from a first order transition in QCD with a large number of colors in the homogeneous regime. The latter is expected to be dominant for a broad range of temperatures and densities. However, it has two major shortcomings: 1/ The (quark) susceptibilities asymptote the wrong values despite the fact that the bulk thermodynamics (pressure, entropy and energy densities) can be adjusted to asymptote the correct values. 2/ The very low temperature phase is likely inhomogeneous. While the latter issue is readily overcome [5], the former issue is more problematic at higher temperature. It goes to the heart of high fermionic charge fluctuations in dense matter and therfore the very interpretation of our charged black hole solutions.

Acknowledgments

This work was supported in part by US-DOE grants DE-FG02-88ER40388 and DE-FG03-97ER4014.

A Non-trivial dilaton-gauge coupling: $c = 4$

In this Appendix, we show that a non-trivial dilaton-gauge coupling affects considerably the formation of the large black hole solution in the model we discussed above.

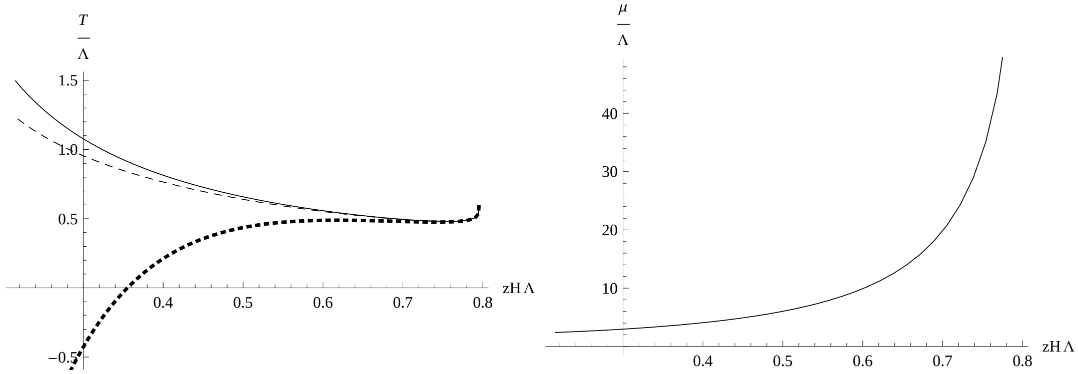

Figure 10: Left: The Hawking temperature at chemical potentials $\mu/\Lambda = 0$ (solid), 1 (dashed), 3.5 (dotted) as a function of the scaled horizon $z_H\Lambda$. Right: The density at $T = 0$.

Fig. 10 shows, that the big black hole branch vanishes completely for densities larger than μ_0 leaving only the unstable solution with an absolute maximum temperature in the IR region ($z_H \to z_w$). In this region, the size of the black hole at a given temperature is insensitive to changes in the charge density. Discarding the unstable small black hole, the range of validity for this setup is dictated by $T \geq T_{min}$, $\mu \leq \mu_0$.

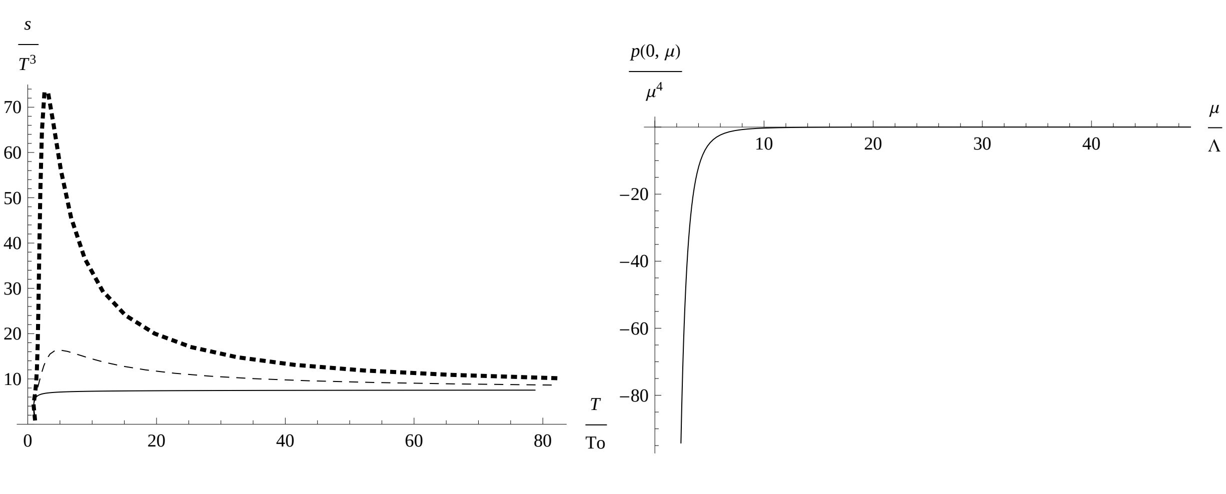

Figure 11: The scaled entropy density s/T^3 at chemical potentials $\mu/\Lambda = 0$ (solid), 1 (dashed), 1.5 (dotted) and the pressure at $T = 0$.

The scaled entropy density, s/T^3, peaks at finite μ around $T = 5T_0$ and the high temperature asymptotic behavior is much slower as in the case of vanishing dilaton-gauge coupling, Fig. 11. The susceptibilities c_4, c_6 do not asymptote for large temperatures. The pressure at $T = 0$ is negative for small μ/Λ and asymptotes to zero for $\mu/\Lambda \geq 10$. Thus, the 'vacuum' solution is stable against the black hole solution at $T = 0$ for all ranges of the chemical potential and no phase transition expected.

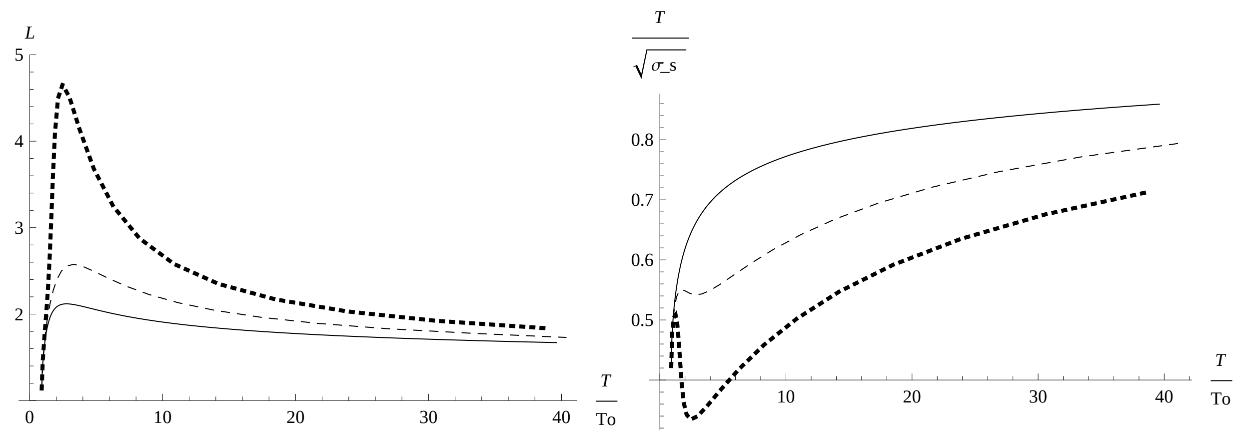

Figure 12: Left: Polyakov line with $\mu/\Lambda = 0$ (solid), 1 (dashed), 1.5 (dotted). Right: Big black hole contribution to the spatial string tension at densities $\mu/\Lambda = 0$ (solid), 1.5 (dashed), 2.5 (dotted). ($w_0 = 1$)

The Polyakov line shows a peak around $T = T_0$ that is enhanced with increasing charge density. Fig. 12 shows the results for the Polyakov line and the spatial string tension with non-trivial dilaton-gauge coupling.

B Warped Model

We discuss the asymptotics of the susceptibilites as obtained for the warped metric proposed in [23] with a charged black hole. At finite temperature and density the metric reads

$$ds^2 = \frac{\mathcal{L}^2}{z^2} e^{0.45\mathrm{GeV}^2 z^2} \left(-f(z)dt^2 + d\vec{x}^{\,2} + \frac{1}{f(z)} dz^2 \right) \tag{59}$$

and we assume that the relation between the horizon z_H and the temperature, density is given by the RN-AdS result [18]

$$z_H = 2 \left(\pi T + \sqrt{\pi^2 T^2 + \frac{4}{3}\gamma^2 \mu^2} \right)^{-1} . \tag{60}$$

The solution (9) is generic and we obtain

$$\mu = \frac{\mathbf{e}}{\mathcal{L}^3}\int_0^{z_H} dx \frac{x}{\mathcal{L}} e^{-0.225\mathrm{GeV}^2 x^2} = -\frac{\mathbf{e}}{\mathcal{L}^4 0.45\mathrm{GeV}^2} e^{0.225\mathrm{GeV}^2 z_H^2}. \tag{61}$$

The charge density is proportional to the charge and using (61) yields

$$n(T,\mu) \propto \mu e^{0.225\mathrm{GeV}^2 z_H^2}. \tag{62}$$

Unlike the improved holographic model, the corresponding susceptibilities vanish as power laws at high temperature,

$$c_2 \propto \frac{1}{T^2} e^{\frac{0.225\mathrm{GeV}^2}{\pi^2 T^2}} \to 0 \tag{63}$$

$$c_4 \propto \frac{1}{T^4} e^{\frac{0.225\mathrm{GeV}^2}{\pi^2 T^2}} \to 0 \tag{64}$$

$$c_6 \propto \left(\# \frac{1}{T^6} + \# \frac{1}{T^4}\right) e^{\frac{0.225\mathrm{GeV}^2}{\pi^2 T^2}} \to 0 \tag{65}$$

This warped and charged black hole cannot be used to model up the fermionic fluctuations in screened QCD.

References

[1] P. de Forcrand, "Simulating QCD at finite density," arXiv:1005.05392 [hep-lat].

[2] M. Fromm and P. de Forcrand, "Nuclear physics from strong coupling QCD," arXiv:0912.2524 [hep-lat].

[3] S. Carignano, D. Nickel and M. Buballa, arXiv:1007.1397 [hep-ph], and references therein.

[4] I. R. Klebanov, "Nuclear Matter In The Skyrme Model," Nucl. Phys. B **262**, 133 (1985); B.Y. Park and V. Vento, "Skyrmion Approach to Finite Density and Temperature," arXiv:0906.3263 [hep-ph], and references therein.

[5] K. Y. Kim, S. J. Sin and I. Zahed, "Dense Holographic QCD in the Wigner-Seitz Approximation," JHEP **0809**, 001 (2008) [arXiv:0712.1582 [hep-th]]; M. Rho, S. J. Sin and I. Zahed, "Dense QCD: a Holographic Dyonic Salt," Phys. Lett. B **689**, 23 (2010) [arXiv:0910.3774 [hep-th]].

[6] U. Gursoy and E. Kiritsis, "Exploring improved holographic theories for QCD: Part I," JHEP **0802**, 032 (2008) [arXiv:0707.1324 [hep-th]].

[7] U. Gursoy, E. Kiritsis and F. Nitti, "Exploring improved holographic theories for QCD: Part II," JHEP **0802**, 019 (2008) [arXiv:0707.1349 [hep-th]].

[8] J. Alanen, K. Kajantie and V. Suur-Uski, "A gauge/gravity duality model for gauge theory thermodynamics," Phys. Rev. D **80**, 126008 (2009) [arXiv:0911.2114 [hep-ph]].

[9] U. Gursoy, E. Kiritsis, L. Mazzanti and F. Nitti, "Holography and Thermodynamics of 5D Dilaton-gravity," JHEP **0905**, 033 (2009) [arXiv:0812.0792 [hep-th]].

[10] S. S. Gubser and F. D. Rocha, arXiv:0911.2898 [hep-th].

[11] C. Charmousis, B. Gouteraux, B. S. Kim, E. Kiritsis and R. Meyer, arXiv:1005.4690 [hep-th].

[12] J. Alanen, K. Kajantie and V. Suur-Uski, "Spatial string tension of finite temperature QCD matter in gauge/gravity Phys. Rev. D **80**, 075017 (2009) [arXiv:0905.2032 [hep-ph]].

[13] U. Gursoy, E. Kiritsis, L. Mazzanti and F. Nitti, “Improved Holographic Yang-Mills at Finite Temperature: Comparison with Nucl. Phys. B **820**, 148 (2009) [arXiv:0903.2859 [hep-th]].

[14] K. Y. Kim, S. J. Sin and I. Zahed, arXiv:hep-th/0608046.

[15] H. Lu, J. w. Mei, C. N. Pope and J. F. Vazquez-Poritz, Phys. Lett. B **673**, 77 (2009) [arXiv:0901.1677 [hep-th]].

[16] T. Faulkner, H. Liu, J. McGreevy and D. Vegh, arXiv:0907.2694 [hep-th].

[17] S. J. Sin and I. Zahed, JHEP **0912**, 015 (2009) [arXiv:0907.1434 [hep-th]].

[18] S. J. Sin, JHEP **0710**, 078 (2007) [arXiv:0707.2719 [hep-th]].

[19] C. R. Allton *et al.*, Phys. Rev. D **71**, 054508 (2005) [arXiv:hep-lat/0501030].

[20] S. K. Ghosh, T. K. Mukherjee, M. G. Mustafa and R. Ray, Phys. Rev. D **73**, 114007 (2006) [arXiv:hep-ph/0603050].

[21] K. Jo, Y. Kim, H. K. Lee and S. J. Sin, JHEP **0811**, 040 (2008) [arXiv:0810.0063 [hep-ph]].

[22] Y. Kim, Y. Matsuo, W. Sim, S. Takeuchi and T. Tsukioka, arXiv:1001.5343 [hep-th].

[23] O. Andreev and V. I. Zakharov, JHEP **0704**, 100 (2007) [arXiv:hep-ph/0611304].

[24] J. M. Maldacena, Phys. Rev. Lett. **80**, 4859 (1998) [arXiv:hep-th/9803002].

[25] O. Andreev, Phys. Rev. Lett. **102**, 212001 (2009) [arXiv:0903.4375 [hep-ph]].

[26] M. Cheng *et al.*, Phys. Rev. D **78**, 034506 (2008) [arXiv:0806.3264 [hep-lat]].